Acta Pharmaceutica Sinica B 2023;13(10):4318–4336

Chinese Pharmaceutical Association
Institute of Materia Medica, Chinese Academy of Medical Sciences

Acta Pharmaceutica Sinica B

www.elsevier.com/locate/apsb
www.sciencedirect.com

ORIGINAL ARTICLE

# An injectable bioactive dressing based on platelet-rich plasma and nanoclay: Sustained release of deferoxamine to accelerate chronic wound healing

**Jiao Zhang[a], Qian Luo[a], Qian Hu[a], Tiantian Zhang[a], Jingyu Shi[b], Li Kong[a], Dehao Fu[c], Conglian Yang[a], Zhiping Zhang[a,d,e,*]**

[a]*Tongji School of Pharmacy, Huazhong University of Science and Technology, Wuhan 430030, China*
[b]*Liyuan Hospital of Tongji Medical College of Huazhong University of Science and Technology, Wuhan 430030, China*
[c]*Department of Orthopaedics, Shanghai General Hospital, Shanghai Jiao Tong University School of Medicine, Shanghai 200080, China*
[d]*National Engineering Research Center for Nanomedicine, Huazhong University of Science and Technology, Wuhan 430030, China*
[e]*Hubei Engineering Research Center for Novel Drug Delivery System, Huazhong University of Science and Technology, Wuhan 430030, China*

Received 22 June 2022; received in revised form 29 August 2022; accepted 20 September 2022

**KEY WORDS**

Injectable hydrogels;
Diabetic wound healing;
Platelet-rich plasma;
Laponite;
Deferoxamine;
Angiogenesis;
Macrophage polarization;

**Abstract** Delayed diabetic wound healing has placed an enormous burden on society. The key factors limiting wound healing include unresolved inflammation and impaired angiogenesis. Platelet-rich plasma (PRP) gel, a popular biomaterial in the field of regeneration, has limited applications due to its non-injectable properties and rapid release and degradation of growth factors. Here, we prepared an injectable hydrogel (DPLG) based on PRP and laponite by a simple one-step mixing method. Taking advantages of the non-covalent interactions, DPLG could overcome the limitations of PRP gels, which is injectable to fill irregular injures and could serve as a local drug reservoir to achieve the sustained release of growth factors in PRP and deferoxamine (an angiogenesis promoter). DPLG has an excellent ability in

*Corresponding author.
E-mail address: zhipingzhang@mail.hust.edu.cn (Zhiping Zhang).

Peer review under the responsibility of Chinese Pharmaceutical Association and Institute of Materia Medica, Chinese Academy of Medical Sciences

https://doi.org/10.1016/j.apsb.2022.11.006

Hypoxia-inducible factor-1-$\alpha$

accelerating wound healing by promoting macrophage polarization and angiogenesis in a full-thickness skin defect model in type I diabetic rats and normal rats. Taken together, this study may provide the ingenious and simple bioactive wound dressing with a superior ability to promote wound healing.



## 1. Introduction

Nonhealing chronic wounds have become a major medical and social burden worldwide. Diabetes is the leading cause of chronic ulcers. According to the latest report from IDF (International Diabetic Federation), 537 million adults are living with diabetes worldwide. The prevalence of diabetes is predicted to rise to 783 million by 2045[1]. Currently, up to 25% of people with diabetes face a lifetime risk of chronic non-healing wounds[2,3]. Diabetic foot ulcers (DFUs) are one of the most prevalent types of chronic wounds, putting diabetics at risk of amputation[4]. At least 68% of these people will die within 5 years[5]. The two main reasons why diabetic wounds are difficult to heal are the unresolved inflammation in the inflammatory phase and the decreased ability of angiogenesis in the proliferative phase[6,7]. Unlike the acute inflammatory response of normal wounds, the inflammation of chronic wounds in diabetic patients is at suboptimal levels, and the inflammatory phase is prolonged indefinitely[6]. Furthermore, the polarization of M1 to M2 macrophages is impaired in diabetic wounds[8]. Many studies have shown that diabetic wounds have impaired angiogenesis during the proliferative phase[7]. The high glucose exposure interferes with the stability of hypoxia-activated transcription factor hypoxia-inducible factor-1-$\alpha$ (HIF-1$\alpha$), a factor that plays an important role in promoting angiogenesis through multiple mechanisms, including the regulation of numerous angiogenesis related genes and generation of angiogenic growth factors[6]. As a result, diabetic wounds cannot upregulate vascular endothelial growth factor (VEGF) in response to soft tissue ischemia, resulting in impaired angiogenesis and wound healing[4,5,9,10]. Therefore, promoting the polarization of macrophages to the M2 phenotype and enhancing angiogenesis in diabetic wounds are crucial to accelerating wound healing. In general, surgical debridement, infection control, and application of wound dressings are part of the routine clinical management of diabetic wounds. However, due to the failure to restore the damaged function of the cells surrounding the wound and the lack of bioactive molecules, the treatment methods are ineffective for many patients[11–13]. Local delivery of growth factors has been proven to be beneficial for wound healing, especially the combined use of multiple growth factors, but the expensive cost limits its widespread clinical application[11,14]. Therefore, it is critical to developing a new therapeutic approach focusing on promoting the polarization of macrophages to the M2 phenotype during the inflammatory phase and accelerating angiogenesis during the proliferative phase for accelerating diabetic chronic wound healing.

Platelet-rich plasma (PRP), especially PRP-derived gel (PG) products, have been widely applied in many regeneration fields, including orthopedic regeneration therapy, oral/maxillofacial surgery, skin wound repair, and hair regeneration due to their superior regeneration ability[15–18]. PRP is rich in a large number of different growth factors and chemokines, such as VEGF, platelet-derived growth factor (PDGF) and basic fibroblast growth factor (bFGF), which can recruit endogenous cells and promote M2 macrophage polarization to suppress inflammatory responses[15]. Platelets in PRP are abundant in sphingosine1-phosphate (S1P), which can also effectively recruit and polarize M2 macrophages[19]. In addition to their regulatory effects on the inflammatory stage, the growth factors mentioned above can also promote angiogenesis in the proliferative phage by promoting endothelial cell migration and proliferation[15]. However, the rapid release of growth factors is one of the most important reasons for limiting the clinical application of PG. Moreover, the released growth factors are rapidly degraded by a large number of enzymes in the wound, so the optimal therapeutic effect cannot be achieved[12,20–23]. Besides, PG is not injectable, resulting in incomplete filling of irregular damage and inconvenient application. Injectable hydrogel dressings are more convenient in practice[24]. Therefore, the key to improving the therapeutic effect of PG lies in improving the injectability of PG and realizing the sustained release of growth factors in PG.

Laponite, an inorganic nanoclay, has been investigated for various biomedical applications due to its biocompatibility, unique disc shape, high surface-to-volume ratio, and surface charge[25,26]. As a 2D biomaterial, laponite itself is endocytosed by cells, causing a wide range of cellular responses and enriching biological processes, including cell proliferation, migration, and extracellular base generation[27]. At the same time, degradation products of laponite [$Na^+$, $Li^+$, $Mg^{2+}$, $Si(OH)_4$] can be absorbed by the human body[28]. $Mg^{2+}$ can improve inflammation, stimulate cell proliferation and promote healing[29]. $Si(OH)_4$ and $Li^+$ can promote the synthesis of type I collagen *via* wnt/$\beta$-catenin signaling pathway[25,30]. More importantly, laponite exhibits unique charging properties. This nanoclay exhibits a dual charge distribution, with negative charges on the particle surface and positive charges along its edges[25]. Therefore, based on its rich surface charge properties, it could generate electrostatic interactions with proteins, as well as other non-covalent interactions such as hydrogen bonds and van der Waals forces, thereby forming hydrogel by the formation of clay-protein-clay bridge[31–34]. This physically cross-linked hydrogel is shear-thinning, therefore it is injectable. Due to its rich charge properties, it could also achieve the sustained release of charged small molecule drugs[35,36].

Inspired by this, we innovatively used laponite to improve the PG gel. The shear-thinning and self-healing hydrogel (PLG) was prepared through non-covalent interactions between laponite and the abundant proteins in PRP (Scheme 1). The hydrogel overcame the limitations of PG gel, which could achieve sustained release of growth factors, and had injectable properties to achieve complete

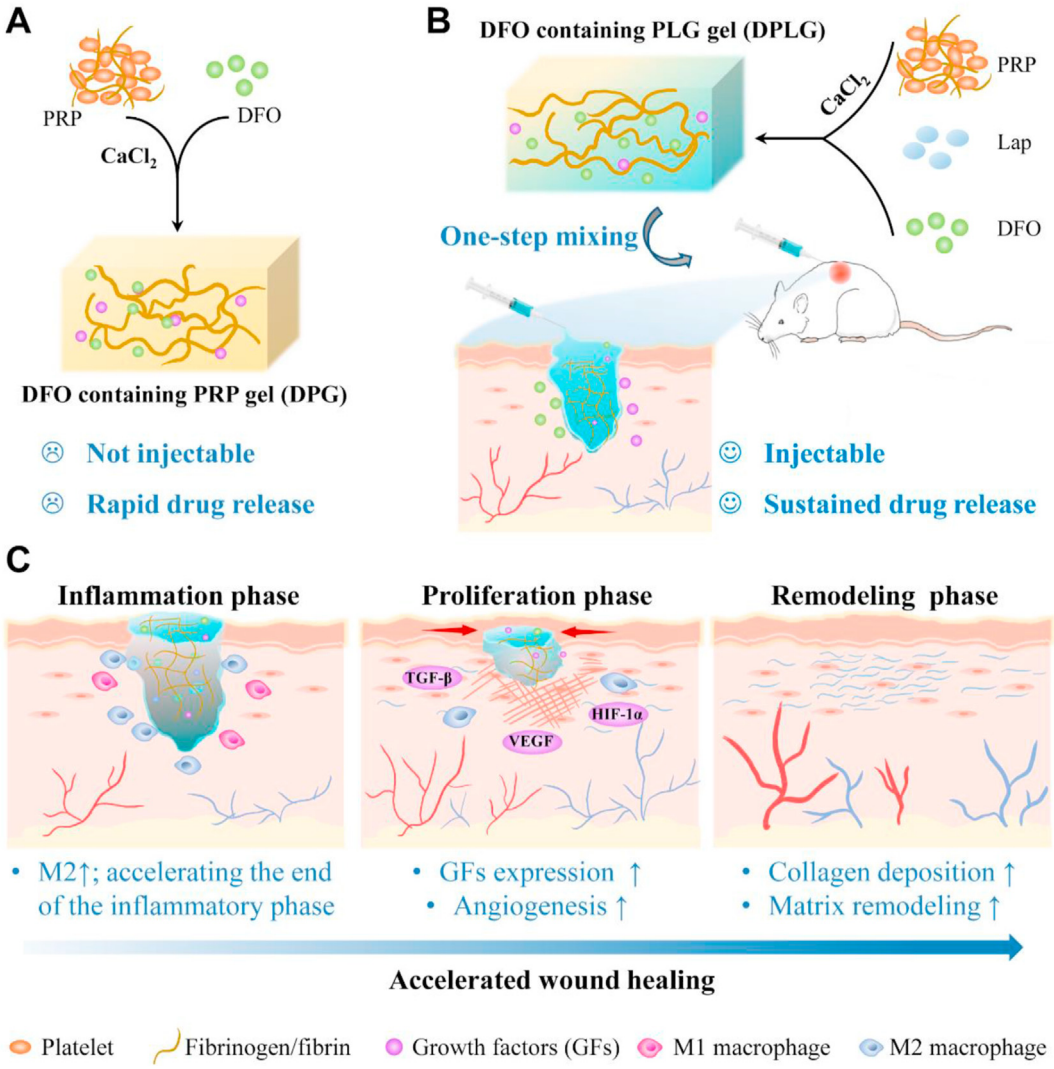


**Scheme 1** Schematic diagram illustrating DPLG hydrogel for diabetic wound healing. (A) The synthetic route of DPG. PG represents the gel formed by pure activated PRP. DPG refers to PG loaded with DFO. DPG is not injectable, and the release rate of GFs and DFO from DPG is very fast. (B) The synthetic route of DPLG. PLG represents the gel formed by activated PRP and Lap (laponite). DPLG refers to PLG loaded with DFO. DPLG is injectable, which could completely fill irregular defects. And it could realize sustained release of GFs and DFO. (C) DPLG could act as a bioactive wound dressing to accelerate diabetic wound healing by acting at different stages of wound healing.

filling of irregular defects. PLG could also serve as a local drug delivery platform to achieve sustained release of other small molecule drugs. Deferoxamine (DFO) was selected as a small molecule drug that could accelerate wound healing by stabilizing HIF-1$\alpha$[9,10,37–42]. DFO containing PLG gel (DPLG) significantly accelerated diabetes wound healing. In general, the hydrogel (DPLG) prepared based on DFO, PRP and laponite in this study has the following advantages: (1) Different from the complex cross-linking process of traditional gels, the preparation of DPLG which requires only one-step mixing is simple. (2) DPLG is injectable, which could fill irregular wounds and is easy to use. (3) It has good biocompatibility, because it does not involve toxic cross-linking agents and the degradation products also have biological activity. (4) It could achieve sustained release of growth factors in PRP to overcome the limitation of clinical common PG gel. (5) It could be used as a drug delivery platform to control drug release and further enhance the clinical therapeutic effect. Therefore, the gel has the potential for clinical application.

## 2. Materials and methods

### 2.1. *Materials*

DFO was purchased from MedChem Express (New jersey, USA). Laponite XLG was obtained from Beijing EAST WEST specialized technology development Co., Ltd (Beijing, China). 3-(4,5-Dimethylthiazol-2-yl)-2,5-diphenyltetrazolium bromide (MTT) was acquired from Biosharp Biotechnology (Hefei, China). Calcein-AM and propidium iodide (PI) were purchased from Invitrogen Corporation (California, USA). Radioimmunoprecipitation assay (RIPA) buffer and bicinchoninic acid

(BCA) protein quantitation kit were obtained from Beyotime Institute of Biotechnology (Shanghai, China). Streptozotocin (STZ) was purchased from Sigma−Aldrich (Missouri, USA).

### 2.2. Cell culture

Human umbilical vein endothelial cell line (HUVEC) and mouse fibroblast cell line (L929) were purchased from Chinese Academy of Science and Technology Cell Bank of China. L929 and HUVEC were cultured in DMEM medium supplemented with 10% FBS, 1% streptomycin, and 100 IU/mL penicillin. All cells were kept in a 37 °C, 5% $CO_2$ incubator.

### 2.3. Animals

Sprague−Dawley (SD) rats (male, 8 weeks old) were brought from Hubei Provincial Center for Disease Prevention and Control (Wuhan, China). All SPF animals were kept in the Animal facility Center, Huazhong University of Science and Technology (HUST). All animal experiments were approved by Institutional Animal Care and Use Committee, HUST (IACUC Number: 2604).

### 2.4. Preparation of PRP

Sodium citrate anticoagulated rat whole blood was centrifuged at 900×*g* (Hunan Xiangyi Laboratory Instrument Development Co., Ltd., L525R, Changsha, China) for 5 min to obtain plasma. Plasma was further centrifuged at 1500×*g* for 15 min to precipitate platelets, and platelets and part of the supernatant were collected and mixed to obtain PRP. PRP was stored at −80 °C.

### 2.5. Preparation of hydrogels

The PG was prepared by mixing 1 mL of PRP and 100 μL of $CaCl_2$ (2.58%, *w*/*w*) at room temperature. The preparation of PLG was achieved by mixing PRP (0.5 mL), calcium chloride (50 μL) and laponite (0.5 mL, 10%, *w*/*w*). In order to obtain DFO-loaded hydrogels (DPG and DPLG), DFO was further added during the hydrogel preparation process. The final DFO loading of DPLG was 600 μg per mL of hydrogel, and the DFO loading of DPG was 600 μg per 500 μL of hydrogel.

### 2.6. In vitro degradation evaluation of hydrogels

Hydrogels with different compositions (*e.g.*, when the volume ratio of PRP and laponite was 2:1, it was recorded as $P_2L_1G$) were weighed and described as the initial weight $W_0$. Then, 0.5 $cm^3$ hydrogels were immersed in 4 mL of PBS and placed on a shaker at 37 °C with a speed of 60 rpm. At pre-set time intervals (1, 4, 12, 24, 36, and 48 h), PBS was removed and the surface moisture of hydrogel was wiped dry, and then the hydrogel was photographed and weighed as $W_t$, respectively. Its morphological changes and mass changes over time were recorded. The relative weight of hydrogels was calculated according to the following Eq. (1):

$$\text{Relative weight } (\%) = W_t/W_0 \times 100 \quad (1)$$

The stability of PLG in plasma was further investigated. The plasma was obtained from fresh rat blood by centrifugation at 2000 rpm (Hunan Xiangyi Laboratory Instrument Development Co., Ltd. , China) for 10 min. The stability of PLG in plasma was investigated according to the method mentioned above.

### 2.7. Characterizations of hydrogels

A tube inversion test was used to test the sol−gel transition, and a 26G syringe needle was used to briefly demonstrate the injectability and self-healing ability of PLG. Scanning electron microscopy (SEM, Quanta 200, FEI, USA) was employed to observe the microstructures of lyophilized PG and PLG. Elemental surface chemistry was characterized by energy dispersive X-ray spectroscopy (EDX). Fourier transform infrared (FTIR) spectrophotometer (AVATAR 360, Thermo, USA) was employed to record the FTIR spectra of the samples. Samples for FTIR analysis were prepared by mixing lyophilized gel and KBr and tableting, with a scan range from 400 to 4000 $cm^{-1}$.

### 2.8. Rheological behavior study

Kinexus Rotational Rheometer (Malvern Instruments, Malvern, UK) was employed to investigate the rheological behavior of hydrogels. Each sample was equilibrated at 25 °C for 5 min by placing in the middle of a 15 mm diameter parallel before testing. The frequency-sweep test of hydrogels was conducted with frequency from 0.1 to 10 Hz and 1% shear strain to record the storage modulus (G') and loss modulus (G"). Viscosity measurements were performed at shear rates ranging from 0.1 to 100 $s^{-1}$ at 25 °C. Recovery experiments were performed to test the self-healing ability of the hydrogels. The self-healing property of PLG and DPLG was measured by applying 1% strain for 2 min followed by 100% strain for 2 min at 1 Hz.

### 2.9. Release profiles of hydrogels

The release behavior of total protein was assessed using a protein quantification kit. 500 μL PG or 1000 μL PLG (containing 500 μL PRP) was placed at the bottom of the low-adsorption EP tube with 0.5 mL of PBS (0.1% sodium azide was added to the media to inhibit bacterial growth and prevent protein degradation). At predetermined time points, all the release media was withdrawn and replaced with 0.5 mL fresh media. BCA kit was used to detect the amount of protein in the release medium. The cumulative release profile was calculated by this Eq. (2):

$$R_t\ (\%) = [A]_t/[A]_{PRP} \times 100 \quad (2)$$

where $[A]_t$ was the cumulative protein release amount at different time intervals, $[A]_{PRP}$ was the total protein in 500 μL activated PRP.

The release behavior of DFO was detected by high performance liquid chromatography (HPLC, UltiMate 3000 Thermo Fisher Scientific machine, Waltham, MA, USA). 500 μL of DPG or 1000 μL of DPLG (with equal amount of DFO) was placed at the bottom of EP tube with 2 mL of PBS. At predetermined time points, all the release media was withdrawn and replaced with 2 mL fresh media. And the collected release media was lyophilized for further analysis. The release medium freeze-dried powder was dispersed in distilled water and combined with 4 mmol/L iron (III) chloride in a 1:1 ratio immediately before analysis *via* HPLC[43]. The mobile phase consisted of acetonitrile and phosphate buffer containing 20 mmol/L EDTA (10:90, *v*/*v*), pH was adjusted to 6.5 and UV detection at 440 nm.

To detect the release of magnesium ions in PLG, PLG was immersed in 5 mL of PBS. After incubation for different times (6, 12, 24, 48, 72 h) at 37 °C, the release media was withdrawn and replaced with 5 mL of fresh media. The detections of $Mg^{2+}$ were performed with atomic absorption spectrometer (AAS, China).

### 2.10. Hemocompatibility assay

The hemolytic properties of hydrogels were evaluated by the hemolysis test. Briefly, the RBCs were obtained from fresh rat blood by centrifugation at 2000 rpm (Hunan Xiangyi Laboratory Instrument Development Co., Ltd.) for 10 min, and then washed with PBS to purify RBCs. The purified RBCs were further diluted into a 5% (*v*/*v*) RBC stock suspension. The 300 μL diluted RBC suspension was mixed with: a) 1 mL PBS as a negative control; b) 1 mL deionized water (DW) as a positive control; c) 50 μL laponite and 1 mL PBS; d) 50 μL PRP and 1 mL PBS; e) 50 μL PLG and 1 mL PBS. After incubation at 37 °C for 2 h, the mixtures were centrifuged for 10 min at 2000 rpm. The hemolytic properties with different treatments were observed *via* a digital camera. Then, the supernatant was collected to measure the absorbance at 540 nm using the microplate reader (Multiskan MK3, Thermo, MA, USA)[44,45]. The percent hemolysis was calculated *via* the following Eq. (3)

$$\text{Hemolysis}\ (\%) = [(A_{\text{sample}} - A_{\text{PBS}}) / (A_{\text{DW}} - A_{\text{PBS}})] \times 100 \quad (3)$$

The hemocompatibility of PLG gel degradation products was further investigated. PBS was used to extract PLG for 24 h to obtain extracts with a concentration of 100%, and the extracts were serially diluted with PBS to obtain 50%, 25% and 10% of the extracts. 300 μL diluted RBC suspension was mixed with: a) 1 mL PBS as a negative control; b) 1 mL 100% extract; c) 1 mL 50% extract; d) 1 mL 25% extract; e) 1 mL 10% extract; f) 1 mL DW as a positive control. The experimental method was consistent with the method mentioned above.

### 2.11. Cytocompatibility assay

The cytocompatibility of PG and PLG was assessed by MTT assay according to the previously reported procedure[45,46]. DMEM medium was used to extract PG or PLG for 24 h to obtain extracts with a concentration of 100%, and were serially diluted with blank DMEM medium to obtain 50%, 25% and 10% of the extracts. L929 or HUVEC cells were seeded in 96-well plates and intervened with different concentrations of extracts for 24 h, and then the cell viability was assessed by MTT assay.

### 2.12. Cell proliferation assay

MTT assay and live/dead staining assay were used to evaluate the proliferative capacity of hydrogels. Briefly, $3 \times 10^3$ L929 were seeded in 96-well plates and intervened with: 1) DMEM as control; 2) 5 μmol/L DFO; 3) 25% PG extract; 4) 25% PLG extract; 5) 25% PG extract and 5 μmol/L DFO; 6) 25% PLG extract and 5 μmol/L DFO, and the cell proliferation was detected by MTT method at predetermined time points (24, 48 and 72 h). To further visualize the proliferation of L929, L929 were seeded in 24-well plates at $2 \times 10^4$ cells per well with DMEM medium and incubated overnight. Then medium was replaced with fresh medium containing various formulations. At predetermined time points (24, 48 and 72 h), cells were washed with PBS, and treated with live/dead staining Kit according to the manufacturer's protocol, and detected under a fluorescent microscope (CKX53, Olympus, Japan).

### 2.13. Migration assay

HUVEC were seeded in 6-well plates with complete medium and incubated at 37 °C until they achieved 90% confluence. Each well was scratched with a 200 μL pipette tip and washed with PBS to remove the floating cells. The original medium was replaced with hydrogel extracts. Cells migration was observed under a light microscope after 24 and 48 h, and the results were analyzed with ImageJ. The experiments were repeated three times.

### 2.14. Tube formation assay

In order to investigate the pro-angiogenic ability of the hydrogels, 50 μL of matrigel was first spread in a 96-well plate and incubated at 37 °C for 1 h to change the matrigel from a liquid state to a gel state. Simultaneously, HUVECs were digested and resuspended with different formulations: 1) DMEM as control; 2) 5 μmol/L DFO; 3) 25% PG extract; 4) 25% PLG extract; 5) 25% PG extract and 5 μmol/L DFO; 6) 25% PLG extract and 5 μmol/L DFO, and then $3 \times 10^4$ cells HUVEC cells were seeded per well. After being cultured for 6 h, the tube formation was recorded by observing and photographing with an optical microscope (CKX53, Olympus, Japan). The result was analyzed by ImageJ software.

### 2.15. Storage stability of DPLG

DPLG was stored at 4 °C for 2 weeks. The stability of stored DPLG and its ability to promote cell proliferation were investigated using the experimental methods described in Sections 2.8 and 2.12.

### 2.16. In vivo biodegradation assay

100 μL PLG gels were implanted subcutaneously in healthy KM mice to investigate the degradation behavior of PLG *in vivo*. The gels were peeled off for photographing and weighing at predetermined time points. The skin around the gel site was fixed in 4% formalin solution for further H&E section analysis.

### 2.17. Evaluation of wound healing ability of hydrogels in a STZ-induced diabetic rat full-thickness skin defect model

#### 2.17.1. Diabetic rat model induced by STZ

STZ was used to induce type I diabetes model. Sprague−Dawley (SD) rats (male, 8 weeks old) were fasted for 16 h, and then intraperitoneally injected with 1% STZ at a dose of 65 mg/kg. The blood glucose level of the rat was monitored every 3 days, and the blood glucose level was maintained above 16.7 mmol/L, indicating that the diabetes model was successfully established.

#### 2.17.2. Diabetic wound repair

The full-thickness skin defect model was established after 14 days of stable blood glucose, and the blood glucose of SD rats was recorded until the complete wound healing. After 14 days, the diabetic rats were anesthetized and shaved, and four circular full-thickness skin defect models were constructed on the back of each rat with a skin biopsy punch (8 mm in diameter)[47,48]. In order to

clarify the advantages of slow release of growth factors, animal experiments were firstly carried out to compare the ability of PG and PLG to promote wound healing. Wounds received the following treatments: 100 μL saline (as a control group), 50 μL PG and 100 μL PLG (The gel volume of PG was halved to ensure that PG contained the same amount of PRP as PLG). In another animal experiment, to further examine the ability of the DFO-loaded gels to promote wound healing, diabetic rats were randomized and received the following four treatments ($n = 6$): 100 μL saline, 50 μL DPG, 100 μL PLG, and 100 μL DPLG (DPG and DPLG contain the same content of DFO.). The wounds on the back of each rat were covered with a Tegaderm film. The hydrogel dressing was changed every 3 days during the treatment period, and the wound area was recorded. The remaining wound area was measured by ImageJ software and the wound closure was calculated by this Eq. (4)

$$\text{Remaining wound area } (\%) = A_t/A_0 \times 100 \quad (4)$$

where $A_0$ is the wound area on Day 0 and $A_t$ is the wound area at different time points.

### 2.18. Histological analysis and immunostaining

Six and fifteen days after surgery, the rats were sacrificed, and tissues from the wound sites were collected and fixed with 4% paraformaldehyde for histological analysis such as hematoxylin and eosin (H&E) staining, Masson's trichrome staining, and picrosirius red staining. Immunohistochemical (IHC) analysis of CD31, HIF-1$\alpha$, VEGF and TGF-$\beta$1 and immunofluorescence (IF) analysis of CD31, $\alpha$-SMA, F4/80, iNOS, CD206 were performed according to standard protocols.

### 2.19. Evaluation of wound healing ability of hydrogels in a rat full-thickness skin defect model

Eight-week-old SD rats were shaved after anesthesia, and 4 wounds were constructed on the back of each rat with a skin biopsy punch (8 mm in diameter). The wounds received three treatments (100 μL saline, 50 μL PG and 100 μL PLG) to demonstrate the advantages of slow release of growth factors caused by the introduction of laponite. In another animal experiment, rats were randomized to receive the following four treatments ($n = 6$): 100 μL saline, 50 μL DPG, 100 μL PLG, and 100 μL DPLG. The wounds were covered with a Tegaderm film. The hydrogel dressing was changed every 2 days during the wound treatment period, and the wound area was recorded. The wound closure was calculated by this Eq. (3)

$$\text{Wound closure rate } (\%) = [A_0 - A_t]/A_0 \times 100 \quad (3)$$

where $A_0$ is the wound area on Day 0 and $A_t$ is the wound area at different time points. On Days 4 and 8, the rats were sacrificed and skin tissues around wound site were collected and fixed in 4% formalin solution for further H&E section analysis and Masson's trichrome staining.

### 2.20. Statistical analysis

All results were described as mean ± standard deviation with at least three independent experiments. One-way ANOVA were used to analyze the differences among multiple groups with Graphpad software. $^{*}P < 0.05$, $^{**}P < 0.01$, and $^{***}P < 0.001$ indicated as statistical difference.

## 3. Results

### 3.1. PLG hydrogel was injectable and could serve as a depot for therapeutic drugs

The preparation process of PLG was simple, and the hydrogel could be formed immediately by one-pot mixing method (Fig. 1B). Briefly, PLG was prepared by mixing and vortexing the FDA-approved biomaterial PRP with the bioactive laponite and a small amount of calcium chloride solution. At the same time, the corresponding PG gel was also prepared for comparative study. According to a previous report[15], by adding calcium chloride or thrombin to PRP, fibrinogen in plasma could be converted into a fibrin network structure, thereby converting PRP from a solution state to a gel-like PG. According to other literature reports[12], PG was prepared by mixing PRP and 2.58% (*w*/*w*) calcium chloride in a volume ratio of 10:1 (Scheme 1A and Supporting Information Fig. S1A). The prepared PG was not injectable and could be pressed which led to the flowing out plasma and the subsequent decreased volume of PG gel (Figs. S1B and S1C). Firstly, we optimized the prescription of PLG gel by adjusting the mixing ratio of PRP and laponite (the volume ratio of PRP to calcium chloride was kept at 10:1). Laponite was first dispersed in deionized water by stirring and adding sodium pyrophosphate to obtain laponite stock solution (10%, *w*/*w*), which was then mixed with PRP according to the proportions shown in Supporting Information Fig. S2A and S2C to investigate the gelation. As shown in Figs. S2B and S2D, when the volume ratios of PRP and laponite were 2:1; 1:1; 1:2; 1:3, they were successfully transformed into a gel state immediately after mixing, and the prepared gels were noted as: $P_2L_1G$, $P_1L_1G$, $P_1L_2G$, $P_1L_3G$. Next, the *in vitro* stability of hydrogels was investigated. All hydrogel samples were immersed in PBS and placed at 37 °C to observe the quality change of hydrogels. $P_2L_1G$ was rapidly degraded with a mass loss of nearly 50% within 1 h, while $P_1L_1G$ was only slightly degraded within 48 h, and the mass of other hydrogels was almost unchanged (Supporting Information Fig. S3A and S3B). Considering that PRP is an FDA-approved and widely used biomaterial, its content in the hydrogel may be proportional to the ability of the hydrogel to promote tissue regeneration. Therefore, unless otherwise specified, PLG referred to $P_1L_1G$ in subsequent experiments. To simulate the effect of *in vivo* ion exchange on PLG, we further investigated the stability of PLG in plasma. The stability of PLG was also well maintained in plasma, indicating that *in vivo* ion exchange did not significantly interfere with the stability of PLG (Figs. S3C and S3D).

The internal morphological structures of lyophilized PG and PLG were further observed by SEM. Fibrin fibers in the PG gel fused longitudinally to form a sheet-like structure (Fig. 1B). Interestingly, in the PLG hydrogel, fiber-like filaments were observed, indicating that PRP was activated and a fibrin network was formed (Fig. 1D). Further analysis by EDX revealed the presence of silicon (Si) and magnesium (Mg) in the PLG gel, two elements derived from laponite (Fig. 1C and E). The presence of laponite in PLG was further confirmed by FTIR spectroscopy. As shown in Fig. 1F, the peaks around 1665 and 1535 $cm^{-1}$ were derived from the amide bond in PRP, and the peaks around 1006

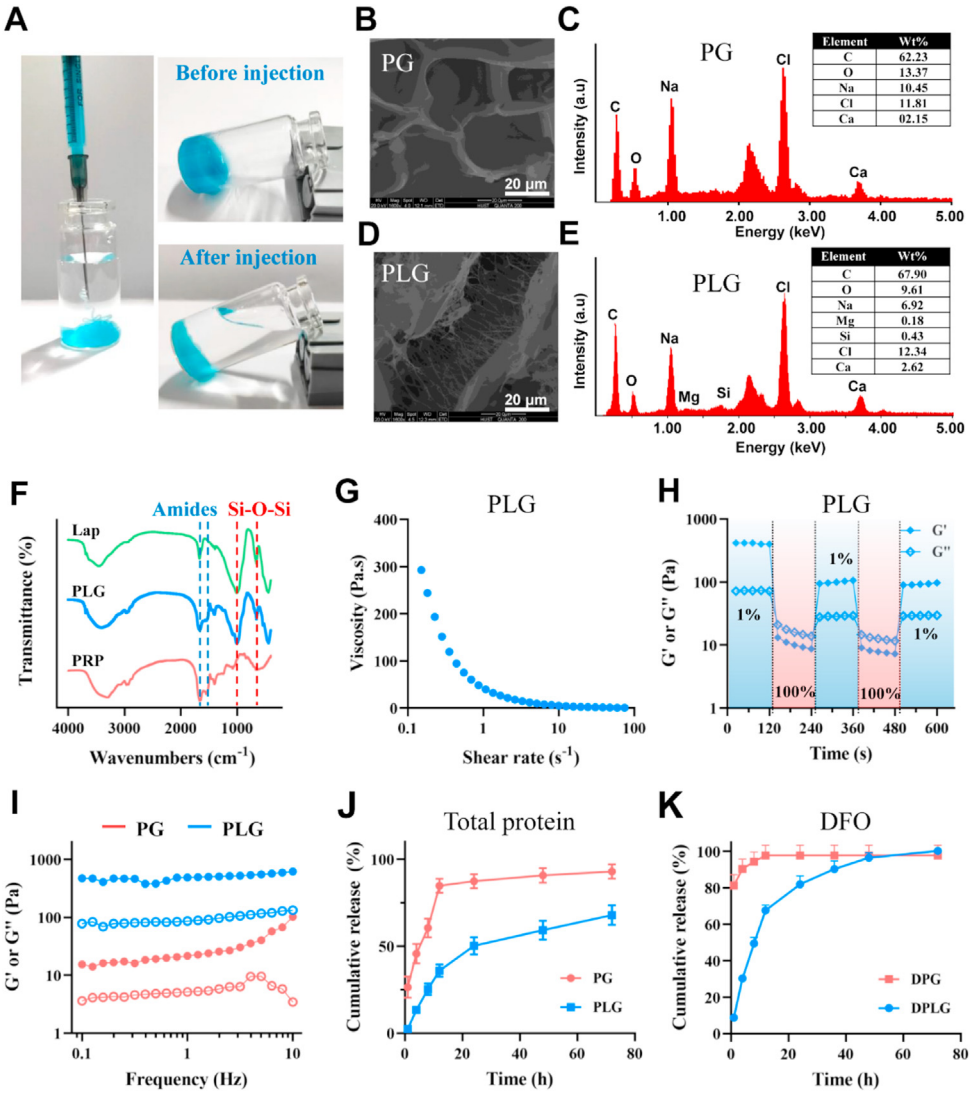


**Figure 1** PLG hydrogel was injectable and could serve as a depot for therapeutic drugs. (A) Photographs of PLG (the gel was stained with methylene blue for better visualization). SEM (B) and EDS (C) analysis of PG. SEM (D) and EDS (E) analysis of PLG. (F) FTIR analysis of Lap (laponite), PLG and PRP. (G) Viscosity over shear rates of PLG. (H) G′ and G″ of PLG during cycling three times of shear strain between 1% and 100%. (I) Storage (G′) modulus (● ) and loss (G″) modulus (○) of PG and PLG. (J) Total protein release profiles of PG and PLG ($n = 3$). (K) DFO release profiles of DPG and DPLG ($n = 3$). Data are reported as mean ± SD.

and 654 $cm^{-1}$ were corresponding to the stretching and bending vibrations of Si−O−Si in laponite, respectively. PLG contained both Si−O−Si peak and amide peak, indicating the presence of PRP and laponite.

Unlike non-injectable PG gels that just rely on covalent polymerization of fibrinogen, PLG could be injected due to its shear-thinning properties and self-healing properties. In PLG gel, non-covalent interactions (including electrostatic interactions, hydrogen bonds, and van der Waals forces, etc.) between protein and clay or between clay and clay may dominate, and this physical interaction could be destroyed during injection, resulting in shear-thinning properties of the gel. These physical interactions will recover spontaneously after injection, thus PLG could be transformed into gel state again. As shown in Fig. 1A (the gel was stained with methylene blue for better visualization), the PLG gel could pass through a 26G syringe, and be back to gel state after injection (Supporting Information Movie 1 and Fig. S4). This property of PLG was very beneficial for clinical applications, as it could assist in the filling of irregular wounds. The shear thinning and self-healing properties of PLG were further confirmed by rheological behavior. The viscosity of PLG gradually decreased with the increasing shear rate, confirming the shear-thinning property of PLG (Fig. 1G). Oscillatory shear study was further employed to demonstrate the self-healing ability of PLG. When a low strain of 1% was applied, the storage modulus G' was greater than the loss modulus G", showing the typical gel state. However, when a high strain of 100% was applied, the storage modulus G' decreased rapidly and was smaller than the loss modulus G", showing a solution state (Fig. 1H). In the frequency sweep test, the G' of both PG and PLG was larger than G", indicating their elastic−dominant properties. In addition, the G' value was related to the

crosslink density, and the larger the G' of the gel, the higher the crosslink density. Therefore, the larger G' of PLG compared to PG might indicate that the cross-linking density of PLG was greater than that of PG (Fig. 1I). We further investigated the rheological properties of the gels loaded with DFO. As shown in Supporting Information Fig. S5, the loading of DFO had no significant effect on the rheological behavior of gels.

Supplementary video related to this article can be found at https://doi.org/10.1016/j.apsb.2022.11.006

Some studies have shown that avoiding the early burst release and achieving local sustained release of growth factors in PRP are essential to improve the therapeutic effect of PRP[12,21]. To investigate the release behavior of growth factors from PG and PLG, we examined the total protein release amount from the hydrogels *in vitro*. As shown in Fig. 1J, the release of PG group rapidly reached 26% within the first 1 h, reached about 85% at 12 h, and then reached a plateau phase. However, the protein release content in PLG was less than 5% within 1 h, and about 36% at 12 h. After that, the protein in the PLG was released continuously at a relatively slow rate. This indicated that the presence of laponite in PLG could facilitate local sustained release of growth factors. It was speculated that the rich surface charge of laponite might interact with various growth factors in PRP, thereby slowing the release of growth factors in PLG gel.

Because the serum half-life of DFO is short, the strong iron lowering effect of DFO may cause side effects[38], and the high local concentration of DFO may cause cytotoxicity[40], the local sustained release of DFO is essential to ensure its safety and therapeutic effect *in vivo*. When DFO was loaded into PG or PLG gels, they were denoted as DPG and DPLG, respectively. Due to the excellent water solubility of DFO and the lack of covalent or non-covalent interaction between DFO and PRP, the DFO in the DPG gel could not be released slowly, and about 80% DFO was released within the first 1 h. On the contrary, only about 10% of DFO loaded in DPLG was released in the first 1 h, and it also maintained a relatively slow-release rate in subsequent time points (Fig. 1K). This may be caused by the electrostatic interaction between the positively charged amine groups of DFO and the abundant negative charges on the surface of laponite. As one of the bioactive degradation products of laponite, the release of $Mg^{2+}$ was also investigated. As shown in Supporting Information Fig. S6, the release amount gradually increased with time, and the concentration of $Mg^{2+}$ in the release medium was about 1.12 mmol/L at 72 h. Several studies have shown that magnesium could dose-dependently promote the proliferation of osteoblasts or vascular endothelial cells in the concentration range of 0−10 mmol/L[49,50]. Therefore, $Mg^{2+}$ released from DPLG might be beneficial to further promote wound healing.

### 3.2. Hydrogels had good biocompatibility and biological activity in vitro

To evaluate the biocompatibility of PLG hydrogel, we first investigated the blood compatibility of PLG. The results show that laponite alone had a certain hemolytic ability due to its abundant charge, but after forming a PLG gel with PRP, its safety was greatly improved (Fig. 2A). Similar to the PBS group, there was almost no hemolysis phenomenon in PLG gel, and the supernatant was clear and transparent. And the degradation products of PLG also showed good blood compatibility (Supporting Information Fig. S7). Next, cytotoxicity evaluation of the hydrogels was performed by MTT method according to a previous report[46]. The cell viability of both HUVEC and L929 was greater than 80% in the tested groups that had been incubated with leachates of PG and PLG for 24 h, which confirmed that both PG and PLG had good cytocompatibility (Fig. 2B and C). The *in vivo* degradation test also showed that PLG gel could degrade over time *in vivo*, and skin H&E slices showed that the gel might trigger a mild inflammatory response in the early stage, but the inflammatory response would automatically subside over time (Supporting Information Fig. S8).

Previous studies have confirmed that the growth factors PDGF, EGF and bFGF in PRP could promote the proliferation of fibroblasts[15]. Laponite and its degradation products could regulate a variety of biological processes including cell proliferation, migration, and extracellular matrix generation[25,27]. As a prolyl-4-hydroxylase (PHD) inhibitor, DFO could increase the stability and activity of HIF-1$\alpha$, thereby increasing angiogenesis[9,37,41,42]. Therefore, the bioactivity of the hydrogels was further investigated through cell proliferation assay, scratch assay and tube formation assay. Firstly, L929 cell line was used to investigate the ability of the hydrogels for promoting cell proliferation. As exhibited in the result of live/dead staining, DPLG showed excellent potential to promote cell proliferation at 72 h, while PLG and DPG achieved moderate and similar proliferative effects (Fig. 2D). MTT quantification results showed the same trend (Fig. 2E). This could be explained by the fact that DPLG contained growth factors derived from PRP, active degradation products derived from laponite, and the bioactive molecule DFO. Scratch assays were further employed to investigate the ability of hydrogels to promote cell migration. DPLG exhibited excellent pro-migration ability, and DPG and PLG also exhibited significantly better ability to promote cell migration than the control group (Fig. 2F and G). As shown in Fig. 2H and I, DPLG and DPG showed significant angiogenesis-promoting effect.

### 3.3. DPLG could accelerate diabetic chronic wound healing

We established a diabetic rat model by a single high-dose intraperitoneal (i.p.) injection of STZ which could destroy pancreatic $\beta$-cells, thereby inhibiting insulin synthesis. Then, full-thickness skin defect was constructed on the back of diabetic rats and treated with different hydrogels as wound dressings or treated with normal saline as a negative control group (Control, Fig. 3A). As shown in Supporting Information Fig. S9, compared with the PG group, wound healing in the PLG-treated group was significantly faster. The wound healing rate in the PLG group was significantly higher than that in control on Days 6 and 9. And the wound healing rate in the PLG group was not only significantly different from that in control, but also significantly higher than that in the PG group on Days 12 and 15. This confirmed that the slow release of growth factors was beneficial for wound healing. As shown in Fig. 3B, PLG, DPG, and DPLG all showed faster wound healing compared to control. Among them, DPLG showed the best wound healing results on Day 15. The wound area was further quantified to calculate the relative wound area (Fig. 3C and D). DPLG showed significantly faster wound closure throughout the treatment period. The relative

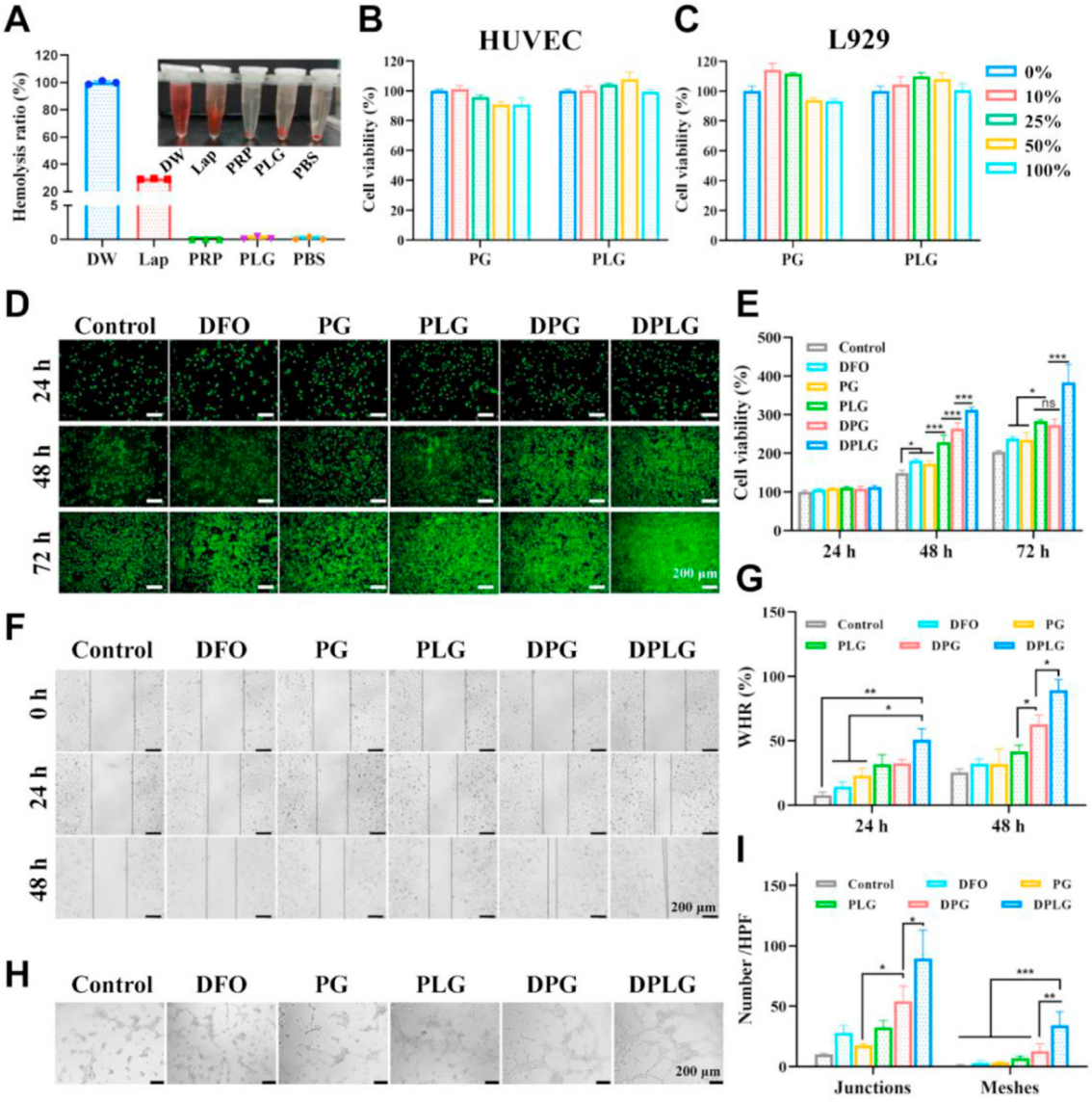


**Figure 2** PLG had good biocompatibility and the loading of DFO further increased its biological activity (A) Hemolysis rate of Lap, PRP and PLG. The inset is the supernatant imaging of RBCs in different treatment groups ($n = 3$). Cell viability of (B) HUVEC and (C) L929 treated with the release media of PLG or PG with different leaching concentrations ($n = 5$). (D) Live/dead staining of fibroblasts (green fluorescence, Calcein-AM indicates live cells; red fluorescence: propidium iodide indicates dead cells). (E) Cell proliferation rate of L929 by MTT ($n = 5$). (F) Representative optical images showing the HUVEC cells migrations in scratch assay. (G) Quantitative analysis of wound closure rate in scratch assay ($n = 3$). (H) Effects of various hydrogels on the tube formation of HUVEC. (I) Quantification of tube junctions and meshes in tube formation assay ($n = 3$). Data are reported as mean ± SD. $^*P < 0.05$, $^{**}P < 0.01$, and $^{***}P < 0.001$. ns, not significant.

wound area of DPLG was only about 18.9%, while the relative wound area of control was about 63.4% on Day 9, indicating that DPLG had a significant advantage in accelerating wound healing in the proliferative phase. At the same time, the relative wound area of DPG was about 41.3%, which was also significantly different from that of control. There were also significant differences between the DPLG and DPG groups, probably because the DPLG could achieve a slow and stable release of growth factors and DFO (Fig. 1J and K), while growth factors and DFO in DPG could only be released rapidly in an uncontrolled manner. On Day 15 after treatment, all three hydrogels showed better wound healing than control. The relative wound area of control remained at about 61.3%, while the wound in the DPLG group was almost completely healed, and the relative wound area was only 6.8%. At this time, the relative wound area of DPG was about 27%, and 41.9% for PLG group. Compared with the DPLG, the wound healing in the PLG was worse, confirming that DFO played an extremely important role in accelerating the healing of diabetic wounds. The ability of DPLG to promote wound healing was better than that of DPG, which confirmed the importance of laponite addition.

### *3.4. DPLG promoted re-epithelialization and collagen deposition at the wound site*

The therapeutic effect of hydrogels on chronic wounds was further revealed by elucidating the microscopic process of diabetic wound healing through histological evaluation. H&E staining showed that

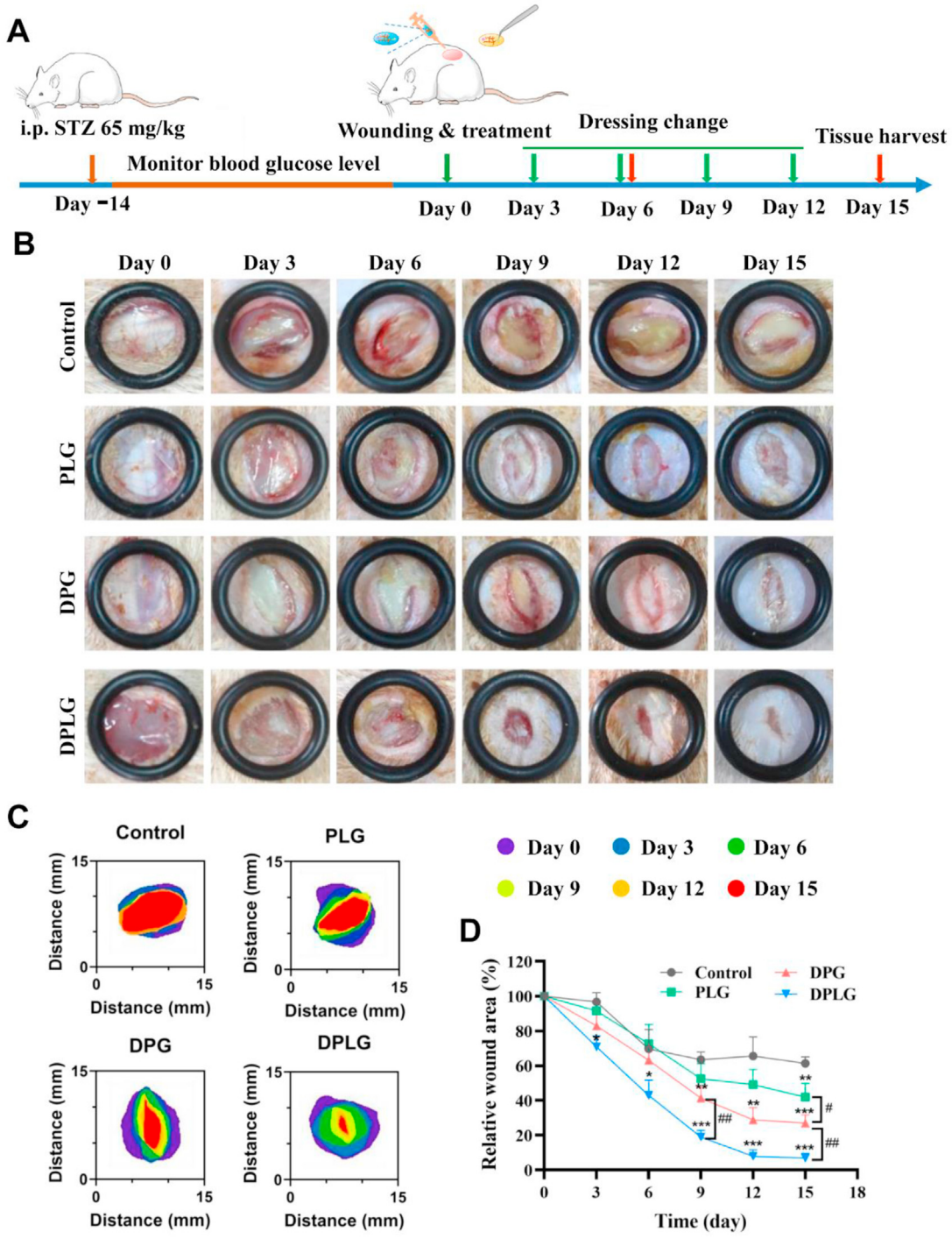


**Figure 3** DPLG hydrogel accelerated wound healing in a full-thickness skin defect of diabetic rats. (A) Schematic diagram illustrating the wound and treatment schedule. (B) The representative photographs of the wound healing process. (C) Schematic diagram of the wound area. (D) Wound healing ratio of the defects ($n = 3$, * indicates significant differences between Control and other groups, # indicates significant differences between the two groups connected by the line segment). Data are reported as mean ± SD. *$P < 0.05$, **$P < 0.01$, and ***$P < 0.001$.

new granulation tissue was formed in DPLG and DPG on Day 6 after treatment (Fig. 4A). Re-epithelialization is an important stage of skin regeneration, typically characterized by thinning and maturation of the epidermal structure of the skin[47]. Epithelial structures were formed in all groups on Day 15. Among them, the epithelial structure was the thinnest and the wound was almost completely closed in DPLG. In addition, skin appendages are functional skin structures that can be used to evaluate the integrity of regenerated skin tissue[47,51]. In the enlarged images in Fig. 4A, the skin appendage regeneration of DPLG group was significantly more than that of the other three groups, showing the best skin function recovery. During the wound healing phase, the deposition

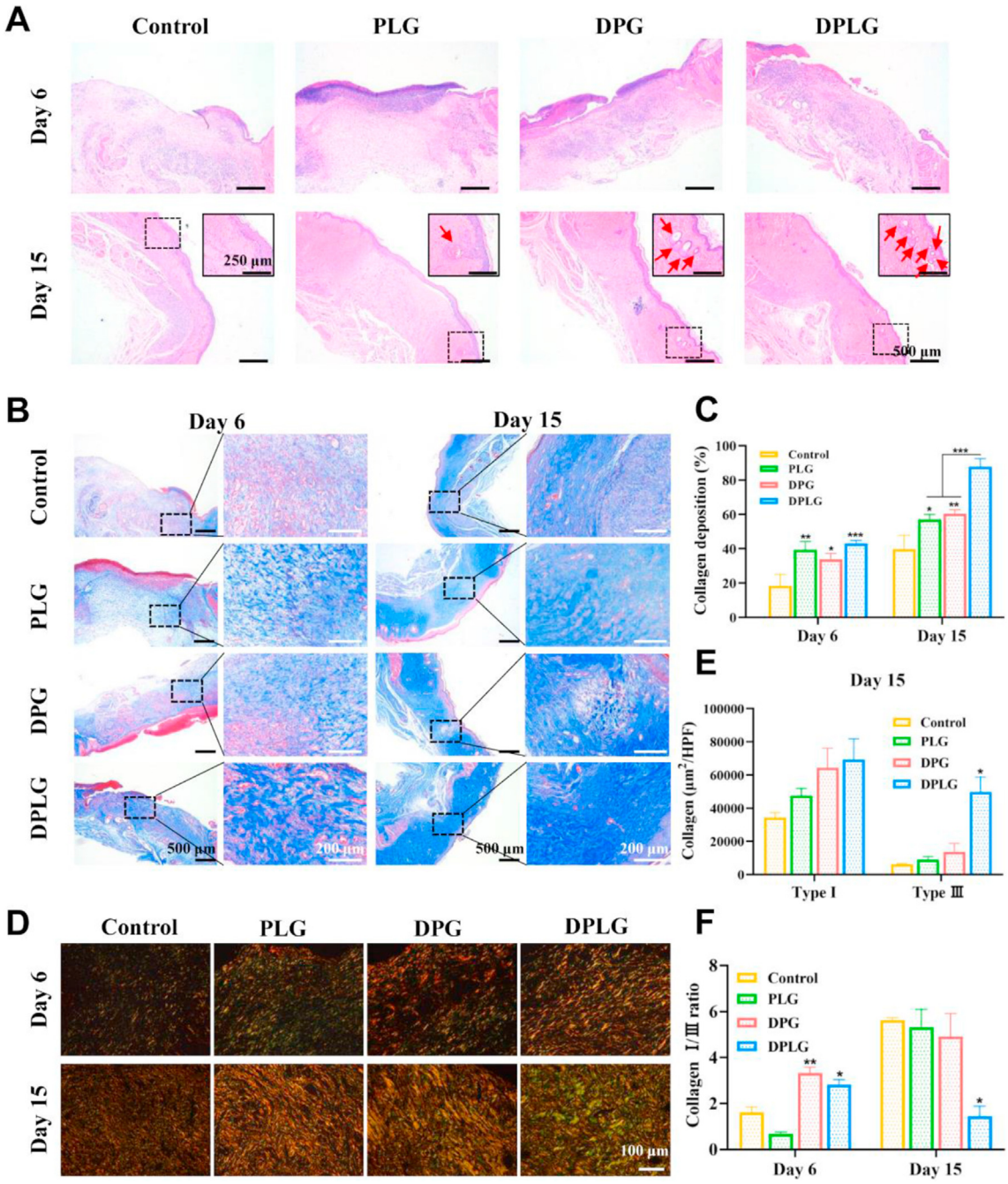


**Figure 4** DPLG promoted re-epithelialization and collagen deposition. (A) H&E staining images of wound sections. Skin appendage structures were indicated by red arrows in the enlarged view. (B) Masson's trichrome staining images of wound sections. (C) Semi-quantitative analysis of collagen deposition ($n = 3$). (D) Representative slides stained with picrosirius red. Type I and type III collagen were stained yellow and green. (E) Semi-quantitative analysis of type I and type III collagen on Day 15 ($n = 3$). (F) Analysis of the collagen I/III ratio on Days 6 and 15 ($n = 3$). Data are reported as mean ± SD. $^{*}P < 0.05$, $^{**}P < 0.01$, and $^{***}P < 0.001$.

and remodeling of collagen facilitate tissue repair and regeneration[48]. Masson's trichrome staining was employed to examine differences in collagen deposition and remodeling during diabetic wound healing. All three hydrogel dressings showed higher amount of blue collagen deposition than control on Days 6 and 15 (Fig. 4B and C). And the collagen deposition area of DPLG reached about 87.8%, which was 2.2 times higher than that of control (about 39.7%) on Day 15 (Fig. 4C). The magnified region of masson staining showed that the collagen fibers in the middle edge of the wound in DPLG were bold and compact, showing a mature phenotype[21]. Collagen types (type I and III) were further distinguished by picrosirius red staining[48,52]. Type I collagen is thicker, and it is the main component of skin tissue, while type III collagen is thinner and is the main component of reticular fibers[53]. The accumulation of both types of collagen fibers facilitates the deposition of extracellular matrix and accelerates wound healing. However, the level of type III collagen in scar tissue is low. The increased deposition of type III collagen during the healing

process facilitates scarless wound healing[48]. In DPG and DPLG groups, the deposition area of yellow or red type I collagen significantly increased on Day 6. The green type III collagen increased slightly in PLG, DPG and DPLG groups (Fig. 4D and Supporting Information Fig. S10). So the ratio of I/III collagen was higher in DPG and DPLG groups (Fig. 4F). Collagen deposition was further increased in DPLG group on Day 15. Compared with other three groups, the increase of type III collagen was more obvious in DPLG. Therefore, although type I collagen and type III collagen were both increased in four groups, the I/III collagen ratio was relatively lower in the DPLG group (Fig. 4D−F). This might be related to the complex self-regulation of the body, but the specific mechanism needs to be further studied.

### 3.5. *DPLG improved suboptimal inflammation levels at the wound site and increased M2 macrophage levels*

Generally speaking, the normal wound healing process can be roughly divided into three stages: inflammatory phase, proliferative phase and tissue remodeling phase[54]. Because of the unresolved inflammation in the inflammatory phase and the decreased ability of angiogenesis in the proliferative phase, diabetic wounds are difficult to heal[6,7]. Therefore, appropriate measures should be taken to regulate the three stages of diabetic wound healing to make it proceed in an orderly manner. In particular, regulating the macrophage phenotype to promote the end of the inflammatory stage and increasing the angiogenesis in the proliferative stage, are beneficial to accelerate wound healing.

As the first of the three stages during wound healing, the main purpose of the inflammatory phase is to prevent infection. Monocytes appear at the injury site and transform into macrophages, first into the pro-inflammatory M1 phenotype to prevent infection. As the inflammatory response progresses, macrophages are polarized into an anti-inflammatory and “pro-healing” M2 phenotype, which help tissue repair by releasing various factors[6]. This polarization of macrophages is critical for ending the inflammatory phase and accelerating wound healing[6,7,55]. The inflammation level of diabetic wounds is at a suboptimal level, in which the polarization of the M1 phenotype to the M2 phenotype is blocked, so that the wound is remained in the inflammatory phase for a long time and cannot enter the proliferative phase[6]. Existing studies suggested that PRP has an immunomodulatory effect, in which S1P contained in platelets could directly recruit endogenous M2 macrophages and polarize the M1 phenotype to the M2 phenotype[19]. At the same time, other growth factors such as VEGF, TGF-$\beta$ and PDGF in PRP also have immunomodulatory effects, which could promote the polarization of M2 macrophage and promote the resolution of inflammation (Fig. 5A)[15].

To investigate inflammation level during diabetic wound healing, the level of TGF-$\beta$1 was examined by IHC staining. TGF-$\beta$ is a multifunctional cytokine that induces the transformation of monocytes into macrophages, thereby enhancing the inflammatory response and tissue debridement[21]. There are three isoforms of TGF-$\beta$ in mammals as TGF-$\beta$1, $\beta$2 and $\beta$3. Among them, TGF-$\beta$1 is the isoform with the most abundant content and the broadest action spectrum in healing wounds[56]. Therefore, TGF-$\beta$1 expression was chosen to further evaluate the wound healing potential of hydrogels. As shown in Fig. 5B and C, the expression of TGF-$\beta$1 in control was significantly lower than that in the treatment groups on Day 6, and the expression level increased on Day 15[57]. The expression levels of TGF-$\beta$1 in DPG and PLG groups were slightly higher than those in control on Day 6, but the TGF-$\beta$1 expression in PLG maintained a higher level on Day 15, while the TGF-$\beta$1 expression in DPG decreased slightly. In the DPLG group, the expression level of TGF-$\beta$1 increased most significantly on Day 6, and decreased significantly on Day 15. This phenomenon might be due to the supplementation of exogenous TGF-$\beta$1 from PRP in treatment groups. Moreover, the DPLG group could better maintain the activity of TGF-$\beta$1 due to the slow release of growth factors. Since the DPLG group synergistically promotes wound healing in multiple directions, making the healing process closer to normal wound healing, the expression of TGF-$\beta$1 decreased significantly in the later stage, which might be caused by the complex self-regulation mechanism of the body. In addition to inflammatory regulation, TGF-$\beta$1 is also associated with extracellular matrix deposition and myofibroblast transformation[21]. Therefore, higher levels of TGF-$\beta$1 in the DPLG-treated group were directly related to faster wound closure.

VEGF could promote angiogenesis by mediating multiple stages of the angiogenic cascade, including vasodilation, endothelial cell migration, and proliferation[58]. In addition to this, VEGF could also modulate the chemotaxis and polarization of macrophages[15]. Several studies have shown that in a full-thickness skin defect model, VEGF expression levels rise immediately after tissue injury and peak on Days 3−7 post-wounding. After about 1 week, with the increase of angiogenesis and the improvement of hypoxia, the expression level of VEGF gradually decreased[58]. Wounds in diabetic animal models induced by STZ show reduced synthesis of VEGF[58]. As shown in Fig. 5D and E, on Day 6, the expression of VEGF in DPG and DPLG groups was significantly increased compared with control. This was mainly caused by the introduction of DFO, as DFO could increase the expression of VEGF by increasing the expression of HIF-1$\alpha$. The highest expression level of VEGF in DPLG might due to the introduction of laponite, which led to the sustained release of exogenous VEGF in PRP, thus maintaining its higher activity. The wounds in the DPLG group had almost completely healed on Day 15, and the reconstruction of blood vessels effectively improved the local hypoxia, so the expression of HIF-1$\alpha$ decreased, resulting in the decrease of the expression of VEGF. However, the wounds in control were still in the proliferation stage on Day 15 due to delayed healing, and the hypoxia was not effectively improved, so the expressions of HIF-1$\alpha$ and VEGF were at higher levels[40].

Next, we examined the ability of the hydrogels to modulate macrophages during wound healing by IF staining analysis of CD206, an important marker of M2 macrophages[48]. As shown in Fig. 5F and G, the number of M2 macrophages in the wounds treated with the three different hydrogel dressing groups increased compared with control, and the increase of M2 macrophages could help to end the inflammatory stage, thus making the wound successfully enter the proliferation stage. The increase of M2 macrophages in DPLG was more obvious on Day 6, which might be related to the higher expression of TGF-$\beta$1 and VEGF. The number of M2 macrophages in three hydrogel treatment groups decreased significantly on Day 15, which might be related to the end of the inflammatory phase and the entry of the proliferation phase.

### 3.6. *DPLG increased HIF-1$\alpha$ expression at wound sites and thereby increased angiogenesis*

Angiogenesis is a necessary condition for wound repair, which could provide necessary oxygen and nutrients to the wound[59].

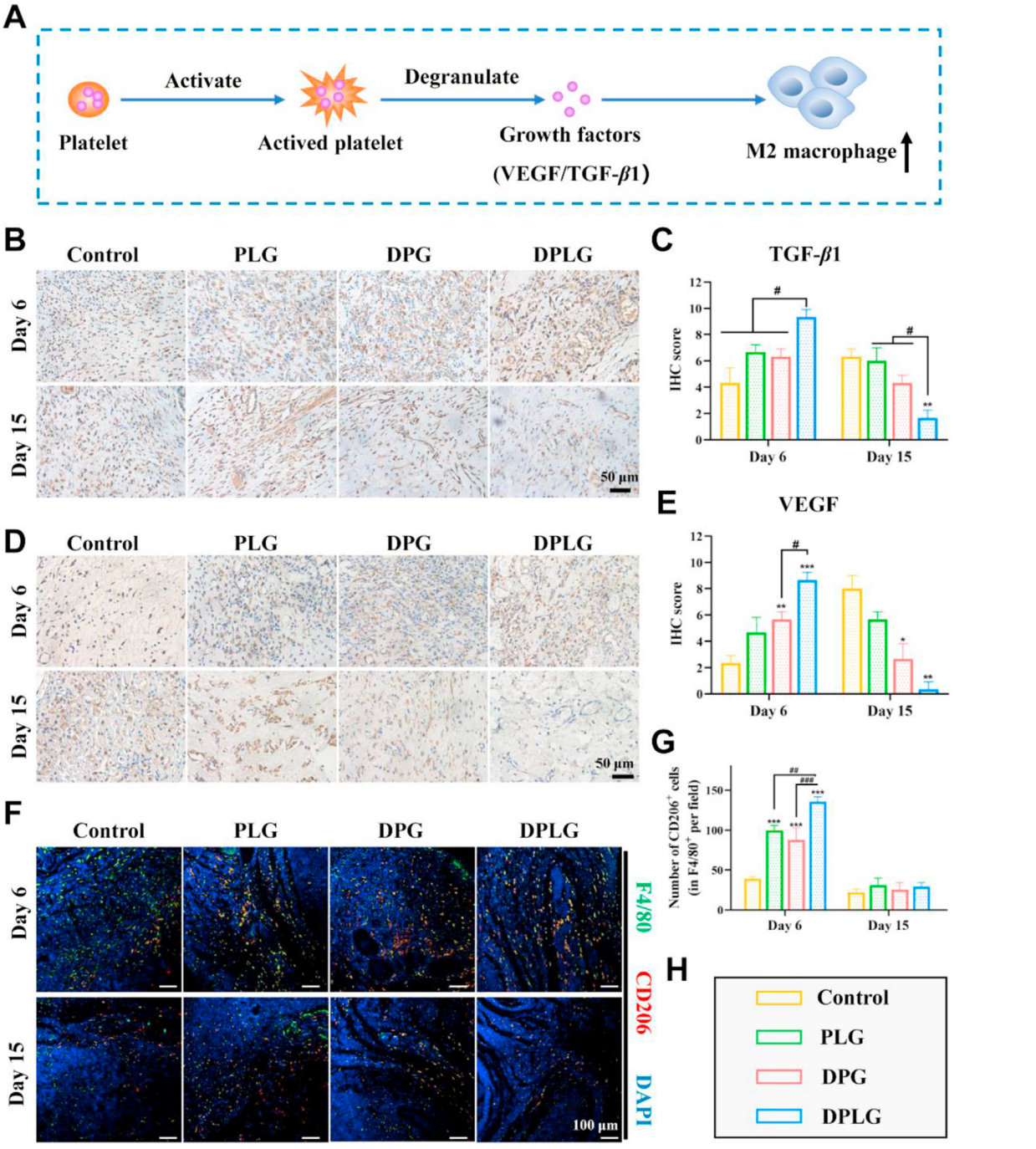


**Figure 5** Hydrogels promoted the polarization of M2 macrophage in the diabetic wound beds. (A) Schematic showing that platelets promote M2 macrophage polarization by releasing growth factors through degranulation. (B) IHC staining of TGF-$\beta$1. (C) The Semi-quantification of IHC staining of TGF-$\beta$1 ($n = 3$). (D) IHC staining of VEGF. (E) The Semi-quantification of IHC staining of VEGF ($n = 3$). (F) Representative images of F4/80 (green) and CD206 (red) immunostaining showed accumulation of M2 macrophages at the wound bed on Days 6 and 15. (G) IF staining analysis of M2 polarization. Data are reported as mean $\pm$ SD (* indicates significant differences between control and other groups, # indicates significant differences between the two groups connected by the line segment.) $^*P < 0.05$, $^{**}P < 0.01$, and $^{***}P < 0.001$.

Insufficient angiogenesis is one of the key factors that make diabetic wounds difficult to heal[7,60]. HIF-1$\alpha$ plays an important role which promotes angiogenesis through multiple mechanisms, including the regulation of numerous angiogenesis related genes and generation of angiogenic growth factors, such as VEGF[7]. The high glucose in diabetic wounds interferes with the stability of HIF-1$\alpha$, resulting in the inability of diabetes wounds to respond to tissue ischemia, thus failing to up regulate VEGF, leading to angiogenesis disorders[5,9,10]. As a stabilizer of HIF-1$\alpha$, DFO could maintain the stability of HIF-1$\alpha$ in the diabetic wound environment, and increase the expression of HIF-1$\alpha$, thereby increasing the expression of VEGF. In conjunction with the VEGF released

from activated platelet, DFO could increase angiogenesis, thereby accelerating wound healing (Fig. 6A). As shown in Fig. 6B and C, on Day 6 after treatment, the expression of HIF-1$\alpha$ was the highest in DPLG, followed by DPG also containing DFO, confirming that the introduction of DFO could increase the expression of HIF-1$\alpha$, and the local sustained release of DFO could play a better effect than the rapid release. The expression of HIF-1$\alpha$ in DPLG was significantly decreased on Day 15, which might be caused by the dominant role of the body's self-regulation. Because with the progress of wound healing, angiogenesis increased and local hypoxia environment improved, the expression of HIF-1$\alpha$ decreased. As a downstream molecule of the HIF-1$\alpha$ pathway, VEGF showed the same trend (Fig. 5D and E). Benefiting from improved expression of HIF-1$\alpha$ and VEGF, angiogenesis in

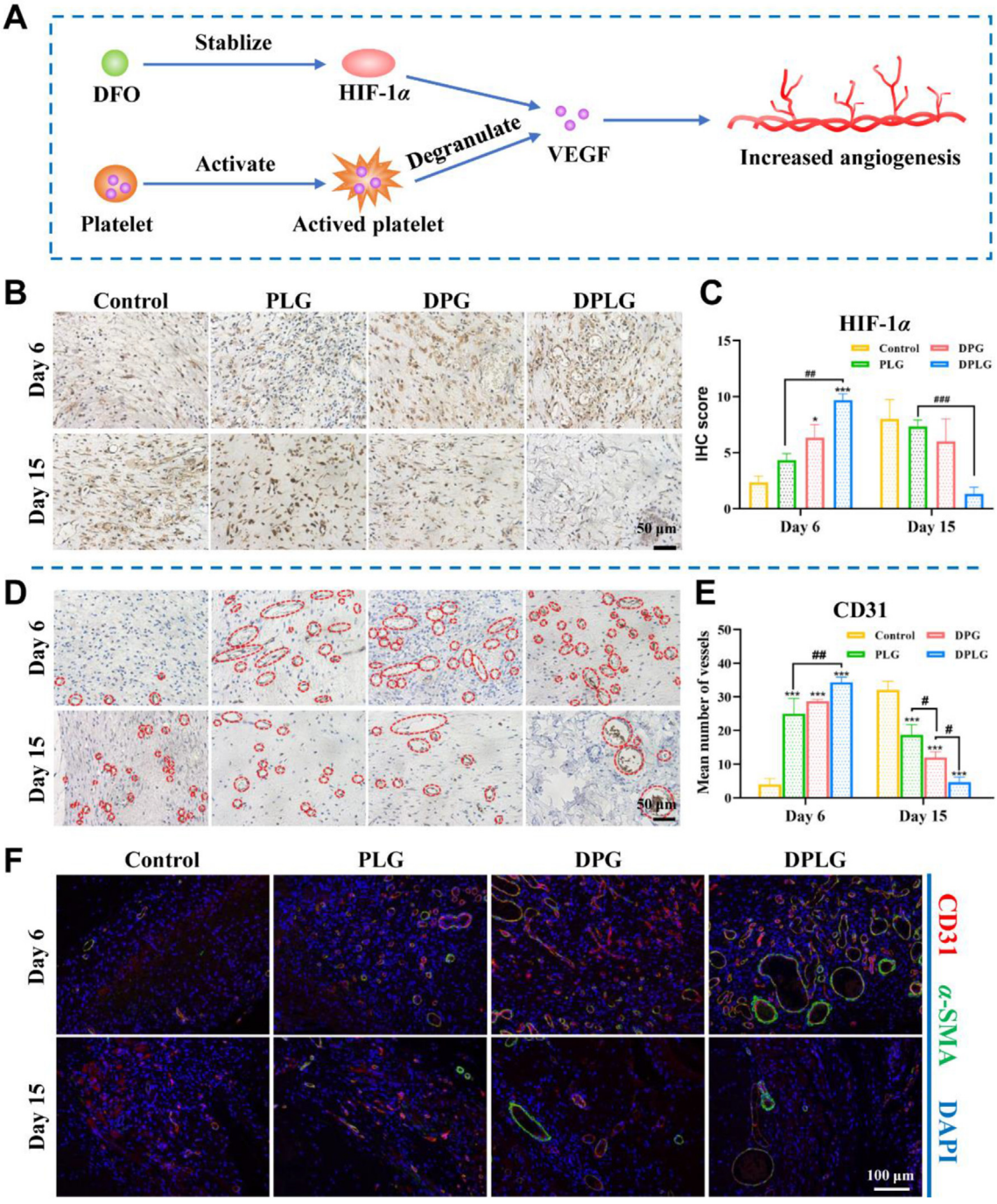


**Figure 6** DPLG increased HIF-1$\alpha$ expression and angiogenesis. (A) Schematic showing that DFO promotes angiogenesis in conjunction with VEGF released from platelet degranulation. (B) IHC staining of HIF-1$\alpha$. (C) Semi-quantification of IHC staining of HIF-1$\alpha$ ($n = 3$). (D) IHC staining of CD31. (E) Semi-quantitative analysis of total blood vessels by IHC staining of CD31 ($n = 3$). (F) IF co-staining for $\alpha$-SMA and CD31 (* indicates significant differences between control and other groups, # indicates significant differences between the two groups connected by the line segment.) Data are reported as mean ± SD. *$P < 0.05$, **$P < 0.01$, and ***$P < 0.001$.

diabetic wounds was improved. As shown in Fig. 6D and E, significantly enhanced neovascularization was shown in all three hydrogel-treated groups on Day 6. Among them, the number of blood vessels per visual field in DPLG was as high as about 34, while the number of blood vessels in control was only about 4. The average number of blood vessels in DPLG was also higher than that in PLG (about 25) and DPG (about 28). The number of blood vessels in control increased significantly on Day 15 after treatment, while the number of blood vessels in the three hydrogel-treated groups decreased. This was because during the remodeling phase, blood vessels would gradually mature to form mature vascular structures with complete functions, while some immature blood vessels disappeared[21]. The tissue regeneration in control was still incomplete on Day 15, and it was still in the proliferation stage, requiring a large number of blood vessels to maintain sufficient oxygen and nutrient supply. Therefore, the number of blood vessels in control was significantly higher than that in the other groups[40,51]. Mature blood vessels have complete vascular structure and function, and nutrients and oxygen are mainly transported by mature blood vessels. Therefore, the maturation of blood vessels is extremely critical for wound repair[40,48]. We further examined mature blood vessels with CD31/$\alpha$-SMA double IF staining. As shown in Fig. 6F, the number of CD31/$\alpha$-SMA double positive blood vessels was the highest in the DPLG-treated group, and luminal structures were larger. These results confirm that the hydrogels indeed increased angiogenesis in diabetic wounds, thereby accelerating wound healing.

### 3.7. *DPLG accelerated common acute wound healing*

Delayed wound healing increases the risk of infection or complications. In addition to diabetic chronic wounds, delayed closure of acute wounds could also exacerbate patient suffering and increase the burden on medical staff[21,61]. In order to investigate the healing effect of the hydrogels in the acute wound model, a full-thickness skin defect model on the back of normal rats was further constructed. Wounds (8 mm in diameter) were constructed on the back of normal rats with a skin biopsy punch, and treated with three different hydrogel dressings or saline (control), respectively. The hydrogel dressings were changed according to the schedule shown in Fig. 7A. Firstly, the ability of PG and PLG to promote wound healing was examined (Supporting Information Fig. S11). The average wound healing rate in PLG group reached about 76% on Day 6, which was significantly different from that in PG group (about 65%) and control (about 58%). The mean wound closure rate in PLG group reached approximately 90% on Day 8, which was significantly better than that in PG group (about 83%) and control (about 77%). The above results fully confirmed that the PLG exhibited a better therapeutic effect than PG, indicating the importance of adding laponite. As shown in Fig. 7B–D, DPLG significantly accelerated wound healing. Semi-quantitative analysis of wound closure rates showed that DPG and DPLG groups had higher rates of healing than control. The healing rate in control reached about 77% on Day 8, while it reached about 73% on Day 4, and about 95% on Day 8 in DPLG group (Fig. 7C). H&E staining results show that the complete re-epithelialization was achieved in DPLG group on Day 8, and a large number of intact hair follicle structures were produced, indicating that not only wound closure was achieved, but also skin function was restored (Fig. 7E). Masson staining showed that all three hydrogel dressings accelerated collagen deposition during acute wound healing, with the most significant increase of collagen deposition in the DPLG group. It was obvious that the collagen in the DPLG group was more mature, and the collagen fibers were bold and arranged in an orderly manner on Day 8 (Fig. 7F and G).

### 3.8. *DPLG had good storage stability*

Preparations with good storage stability will be more conducive to clinical applications. The storage stability of DPLG was investigated, and the results show that after two weeks of storage, the rheological properties of DPLG did not change significantly, and it still had shear-thinning and self-healing abilities. At the same time, it was confirmed by L929 proliferation assay that the stored DPLG retained a good biological activity (Supporting Information Fig. S12).

## 4. Discussion

Delayed healing of diabetic chronic wounds is a dilemma faced by up to 25% of diabetic patients[2], and the existing clinical care methods cannot achieve satisfactory therapeutic effects[11–13]. There are many reasons why diabetic wounds are difficult to heal, among which the unresolved inflammation in the inflammatory phase and the decreased ability of angiogenesis in the proliferative phase are two very important reasons[6,7]. Due to the superior regeneration ability of PRP, it has been widely studied and applied in many regeneration fields[15–17]. After being activated by calcium chloride and/or thrombin, the activated platelets in PRP will immediately degranulate to secret a large number of growth factors. At the same time, fibrinogen in the plasma is activated to convert into fibrin networks, thereby forming a gel structure to provide a moist environment that is more conducive to healing[11,62]. However, this PG has poor mechanical properties, which is not injectable to completely fill the irregular wound bed, and the contained growth factors are rapidly released and degraded by the protease-rich wound environment, making the treatment less effective[11,63]. Therefore, in order to overcome the limitations of PG, we introduced laponite, a nanosilicate with unique disc shape, high surface-to-volume ratio and abundant surface charge in this work to prepare a novel hydrogel PLG. Based on the fibrin network structure generated by the activation of calcium chloride and the non-covalent interaction of laponite with PRP, PLG possessed shear-thinning and self-healing properties and could be injected to fill irregular defects. PLG could achieve the sustained release of growth factors in PRP. In addition to serving as a bioactive hydrogel dressing by itself, PLG could also act as a local drug reservoir, loading drug molecules and controlling their release behavior. In this study, the small molecule HIF-1$\alpha$ inhibitor DFO was loaded within PLG (DPLG), which could help wound repair by stabilizing HIF-1$\alpha$ and increasing angiogenesis. Through electrostatic adsorption, DFO could be slowly released from DPLG, thereby reducing side effects and accelerating wound healing together with PRP. DPLG effectively overcame the limitations of non-injectable and burst release of PG itself, showing better therapeutic effect than DPG in wound repair model. Sustained release of growth factors and platelet-derived S1P could modulate the macrophage phenotype, promote the end of the inflammatory phase and drive the healing process into the proliferative phase. Growth factors and DFO synergistically improved angiogenesis during the proliferative phase. Ultimately, it achieved the purpose of promoting re-epithelialization, accelerating

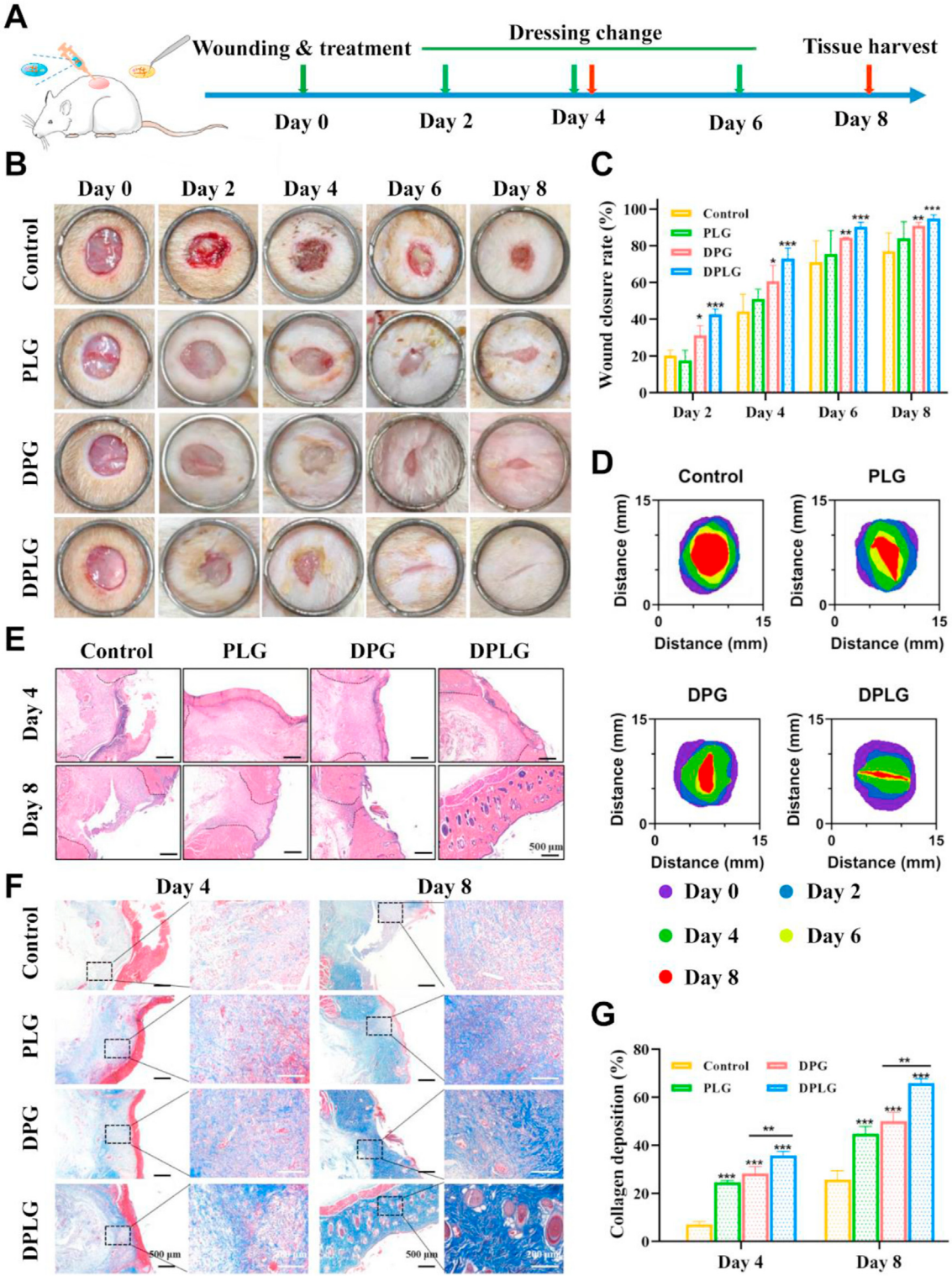


**Figure 7** DPLG hydrogel accelerated wound healing in a full-thickness skin defect of normal rats. (A) Schematic diagram illustrating the wound and treatment schedule in normal rats. (B) The representative photographs of the wound healing process. (C) Wound healing ratio of the defects ($n = 3$). (D) Analysis of wound healing trace. (E) H&E staining images of wound sections. (F) Masson's trichrome staining images of wound sections. (G) Semi-quantitative analysis of collagen deposition in wounds ($n = 3$). Data are reported as mean ± SD. $^{*}P < 0.05$, $^{**}P < 0.01$, and $^{***}P < 0.001$.

wound closure and promoting the recovery of skin function. DPLG has the potential for clinical translation because of its simple preparation and superior wound healing ability, and is of great significance for alleviating the pain of patients and reducing the medical burden on society.

In future studies, the specific mechanism of gel formation by PRP and laponite will be further investigated. And further experiments will be carried out on large animal models such as pigs. The skin structure and function of these animals are more similar to that of humans, which could further verify the safety and efficacy of this DPLG treatment. In addition, based on the fact that PRP itself also plays an important role in the field of bone repair, the application potential of DPLG in bone defect repair will be evaluated to broaden the application scope of this hydrogel.

## 5. Conclusions

Overall, we constructed a novel injectable hydrogel dressing DPLG based on PRP and laponite which improved the current popular biomaterial PRP in regeneration field by ingenious design and in a simple way, so that it could better exert its value in the field of tissue regeneration. Commonly used wound dressings are mainly hydrocolloids, hydrogels and foams, which lack bioactive molecules to modulate the wound microenvironment. DPLG contains both the active ingredients PRP and DFO, which demonstrate a pleasing effect on wound healing. Although some growth factor products are used to accelerate wound healing, they are expensive and easily inactivated, while DPLG is less expensive and could maintain the activity of growth factors better, resulting in better therapeutic effects. Therefore, DPLG has the advantages of simple preparation, low cost, good biosafety and satisfactory effects, which provides a new nursing option for wound repair. This research is of great significance for alleviating the pain of patients and reducing the medical burden on society.

## Acknowledgments

This work was supported by funds from National Natural Science Foundation of China (82173760, 32101144, China) and Program for HUST Academic Frontier Youth Team (2018QYTD13, China).

## Author contributions

Zhiping Zhang supervised the subject. Jiao Zhang designed the study and experiments. Jiao Zhang and Qian Luo performed the experiments. Qian Hu, Tiantian Zhang, and Jingyu Shi contributed to *in vivo* wound healing evaluation. Jiao Zhang wrote the draft manuscript. Zhiping Zhang, Conglian Yang, Li Kong and Dehao Fu discussed the results and edited the manuscript. All of the authors have read and approved the final manuscript.

## Conflicts of interest

The authors have no conflicts of interest to declare.

## Appendix A. Supporting information

Supporting data to this article can be found online at https://doi.org/10.1016/j.apsb.2022.11.006.

## References

1. International Diabetes Federation. *IDF diabetes atlas (IDF)*, vol. 10; 2021. Available from, https://www.idf.org/.
2. He S, Walimbe T, Chen H, Gao K, Kumar P, Wei Y, et al. Bioactive extracellular matrix scaffolds engineered with proangiogenic proteoglycan mimetics and loaded with endothelial progenitor cells promote neovascularization and diabetic wound healing. *Bioact Mater* 2022;**10**:460–73.
3. Wu H, Yang P, Li A, Jin X, Zhang Z, Lv H. *Chlorella* sp.-ameliorated undesirable microenvironment promotes diabetic wound healing. *Acta Pharm Sin B* 2023;**13**:410–24.
4. Qi X, Xiang Y, Cai E, You S, Gao T, Lan Y, et al. All-in-one: harnessing multifunctional injectable natural hydrogels for ordered therapy of bacteria-infected diabetic wounds. *Chem Eng J* 2022;**439**:135691.
5. Chen H, Cheng Y, Tian J, Yang P, Zhang X, Chen Y, et al. Dissolved oxygen from microalgae-gel patch promotes chronic wound healing in diabetes. *Sci Adv* 2020;**6**:eaba4311.
6. Sawaya AP, Stone RC, Brooks SR, Pastar I, Jozic I, Hasneen K, et al. Deregulated immune cell recruitment orchestrated by FOXM1 impairs human diabetic wound healing. *Nat Commun* 2020;**11**:4678.
7. Veith AP, Henderson K, Spencer A, Sligar AD, Baker AB. Therapeutic strategies for enhancing angiogenesis in wound healing. *Adv Drug Deliv Rev* 2019;**146**:97–125.
8. Qian Y, Zheng Y, Jin J, Wu X, Xu K, Dai M, et al. Immunoregulation in diabetic wound repair with a photoenhanced glycyrrhizic acid hydrogel scaffold. *Adv Mater* 2022;**34**:e2200521.
9. Botusan IR, Sunkari VG, Savu O, Catrina AI, Grünler J, Lindberg S, et al. Stabilization of HIF-1alpha is critical to improve wound healing in diabetic mice. *Proc Natl Acad Sci U S A* 2008;**105**:19426–31.
10. Thangarajah H, Yao D, Chang EI, Shi Y, Jazayeri L, Vial IN, et al. The molecular basis for impaired hypoxia-induced VEGF expression in diabetic tissues. *Proc Natl Acad Sci U S A* 2009;**106**:13505–10.
11. Eming SA, Martin P, Tomic-Canic M. Wound repair and regeneration: mechanisms, signaling, and translation. *Sci Transl Med* 2014;**6**:265sr6.
12. Qian Z, Wang H, Bai Y, Wang Y, Tao L, Wei Y, et al. Improving chronic diabetic wound healing through an injectable and self-healing hydrogel with platelet-rich plasma release. *ACS Appl Mater Interfaces* 2020;**12**:55659–74.
13. Shen YI, Cho H, Papa AE, Burke JA, Chan XY, Duh EJ, et al. Engineered human vascularized constructs accelerate diabetic wound healing. *Biomaterials* 2016;**102**:107–19.
14. Llopis-Hernández V, Cantini M, González-García C, Cheng Zhe A, Yang J, Tsimbouri Penelope M, et al. Material-driven fibronectin assembly for high-efficiency presentation of growth factors. *Sci Adv* 2016;**2**:e1600188.
15. Etulain J. Platelets in wound healing and regenerative medicine. *Platelets* 2018;**29**:556–68.
16. Wang S, Li Y, Li S, Yang J, Tang R, Li X, et al. Platelet-rich plasma loaded with antibiotics as an affiliated treatment for infected bone defect by combining wound healing property and antibacterial activity. *Platelets* 2021;**32**:479–91.
17. Gentile P, Garcovich S. Autologous activated platelet-rich plasma (AA-PRP) and non-activated (A-PRP) in hair growth: a retrospective, blinded, randomized evaluation in androgenetic alopecia. *Expet Opin Biol Ther* 2020;**20**:327–37.
18. Conde-Montero E, de la Cueva Dobao P, Martínez González JM. Platelet-rich plasma for the treatment of chronic wounds: evidence to date. *Chron Wound Care Manag Res* 2017;**4**:107–20.
19. Pan X, Yuan S, Xun X, Fan Z, Xue X, Zhang C, et al. Long-term recruitment of endogenous M2 macrophages by platelet lysate-rich plasma macroporous hydrogel scaffold for articular cartilage defect repair. *Adv Healthc Mater* 2022;**11**:e2101661.
20. Tao J, Liu H, Wu W, Zhang J, Liu S, Zhang J, et al. 3D-printed nerve conduits with live platelets for effective peripheral nerve repair. *Adv Funct Mater* 2020;**30**:2004272.

21. Zhang X, Yao D, Zhao W, Zhang R, Yu B, Ma G, et al. Engineering platelet-rich plasma based dual-network hydrogel as a bioactive wound dressing with potential clinical translational value. *Adv Funct Mater* 2020;**31**:2009258.
22. Jiang T, Ma Y, Xu X, Ji Q, Feng M, Cheng C, et al. Enzyme-instructed hybrid nanogel/nanofiber oligopeptide hydrogel for localized protein delivery. *Acta Pharm Sin B* 2021;**11**:2070−9.
23. Liu T, Chen M, Fu J, Sun Y, Lu C, Quan G, et al. Recent advances in microneedles-mediated transdermal delivery of protein and peptide drugs. *Acta Pharm Sin B* 2021;**11**:2326−43.
24. Qi X, Huang Y, You S, Xiang Y, Cai E, Mao R, et al. Engineering robust Ag-decorated polydopamine nano-photothermal platforms to combat bacterial infection and prompt wound healing. *Adv Sci* 2022;**9**:e2106015.
25. Gaharwar AK, Cross LM, Peak CW, Gold K, Carrow JK, Brokesh A, et al. 2D nanoclay for biomedical applications: regenerative medicine, therapeutic delivery, and additive manufacturing. *Adv Mater* 2019;**31**: e1900332.
26. Han L, Lu X, Liu K, Wang K, Fang L, Weng LT, et al. Mussel-inspired adhesive and tough hydrogel based on nanoclay confined dopamine polymerization. *ACS Nano* 2017;**11**:2561−74.
27. Carrow JK, Cross LM, Reese RW, Jaiswal MK, Gregory CA, Kaunas R, et al. Widespread changes in transcriptome profile of human mesenchymal stem cells induced by two-dimensional nanosilicates. *Proc Natl Acad Sci U S A* 2018;**115**:E3905−13.
28. Gaharwar AK, Mihaila SM, Swami A, Patel A, Sant S, Reis RL, et al. Bioactive silicate nanoplatelets for osteogenic differentiation of human mesenchymal stem cells. *Adv Mater* 2013;**25**:3329−36.
29. Guo Z, Zhang Z, Zhang N, Gao W, Li J, Pu Y, et al. A $Mg^{2+}$/polydopamine composite hydrogel for the acceleration of infected wound healing. *Bioact Mater* 2022;**15**:203−13.
30. Xavier JR, Thakur T, Desai P, Jaiswal MK, Sears N, Cosgriff-Hernandez E, et al. Bioactive nanoengineered hydrogels for bone tissue engineering: a growth-factor-free approach. *ACS Nano* 2015;**9**: 3109−18.
31. Gaharwar AK, Avery RK, Assmann A, Paul A, McKinley GH, Khademhosseini A, et al. Shear-thinning nanocomposite hydrogels for the treatment of hemorrhage. *ACS Nano* 2014;**8**:9833−42.
32. Shi P, Kim YH, Mousa M, Sanchez RR, Oreffo ROC, Dawson JI. Self-assembling nanoclay diffusion gels for bioactive osteogenic microenvironments. *Adv Healthc Mater* 2018;**7**:e1800331.
33. Dawson JI, Kanczler JM, Yang XB, Attard GS, Oreffo ROC. Clay gels for the delivery of regenerative microenvironments. *Adv Mater* 2011; **23**:3304−8.
34. Cross LM, Carrow JK, Ding X, Singh KA, Gaharwar AK. Sustained and prolonged delivery of protein therapeutics from two-dimensional nanosilicates. *ACS Appl Mater Interfaces* 2019;**11**:6741−50.
35. Wu Y, Li K, Kong L, Tang Y, Li G, Jiang W, et al. Functional LAPONITE nanodisks enable targeted anticancer chemotherapy *in vivo*. *Bioconjugate Chem* 2020;**31**:2404−12.
36. Lee CS, Hwang HS, Kim S, Fan J, Aghaloo T, Lee M. Inspired by nature: facile design of nanoclay-organic hydrogel bone sealant with multifunctional properties for robust bone regeneration. *Adv Funct Mater* 2020;**30**:2003717.
37. Zhang X, Li Y, Ma Z, He D, Li H. Modulating degradation of sodium alginate/bioglass hydrogel for improving tissue infiltration and promoting wound healing. *Bioact Mater* 2021;**6**:3692−704.
38. Duscher D, Trotsyuk AA, Maan ZN, Kwon SH, Rodrigues M, Engel K, et al. Optimization of transdermal deferoxamine leads to enhanced efficacy in healing skin wounds. *J Control release* 2019;**308**: 232−9.
39. Duscher D, Neofytou E, Wong VW, Maan ZN, Rennert RC, Inayathullah M, et al. Transdermal deferoxamine prevents pressure-induced diabetic ulcers. *Proc Natl Acad Sci U S A* 2015;**112**:94−9.
40. Kong L, Wu Z, Zhao H, Cui H, Shen J, Chang J, et al. Bioactive injectable hydrogels containing desferrioxamine and bioglass for diabetic wound healing. *ACS Appl Mater Interfaces* 2018;**10**: 30103−14.
41. Stegen S, van Gastel N, Eelen G, Ghesquiere B, D'Anna F, Thienpont B, et al. HIF-1alpha promotes glutamine-mediated redox homeostasis and glycogen-dependent bioenergetics to support post-implantation bone cell survival. *Cell Metabol* 2016;**23**:265−79.
42. Semenza GL. Hypoxia-inducible factors in physiology and medicine. *Cell* 2012;**148**:399−408.
43. Li A, Liang C, Xu L, Wang Y, Liu W, Zhang K, et al. Boosting 5-ALA-based photodynamic therapy by a liposomal nanomedicine through intracellular iron ion regulation. *Acta Pharm Sin B* 2021;**11**:1329−40.
44. Lin A, Liu Y, Zhu X, Chen X, Liu J, Zhou Y, et al. Bacteria-responsive biomimetic selenium nanosystem for multidrug-resistant bacterial infection detection and inhibition. *ACS Nano* 2019;**13**: 13965−84.
45. Liu Y, Zhuang B, Yuan B, Zhang H, Li J, Wang W, et al. Predatory bacterial hydrogels for topical treatment of infected wounds. *Acta Pharm Sin B* 2023;**13**:315−26.
46. Huang L, Li Y, Du Y, Zhang Y, Wang X, Ding Y, et al. Mild photothermal therapy potentiates anti-PD-L1 treatment for immunologically cold tumors *via* an all-in-one and all-in-control strategy. *Nat Commun* 2019;**10**:4871.
47. Zhou W, Duan Z, Zhao J, Fu R, Zhu C, Fan D. Glucose and MMP-9 dual-responsive hydrogel with temperature sensitive self-adaptive shape and controlled drug release accelerates diabetic wound healing. *Bioact Mater* 2022;**17**:1−17.
48. Wang K, Dong R, Tang J, Li H, Dang J, Zhang Z, et al. Exosomes laden self-healing injectable hydrogel enhances diabetic wound healing via regulating macrophage polarization to accelerate angiogenesis. *Chem Eng J* 2022;**430**:132664.
49. Shen X, Zhang Y, Ma P, Sutrisno L, Luo Z, Hu Y, et al. Fabrication of magnesium/zinc-metal organic framework on titanium implants to inhibit bacterial infection and promote bone regeneration. *Biomaterials* 2019;**212**:1−16.
50. Daniela B, Anna N, Andrzej M, Jeanette AMM. Magnesium and microvascular endothelial cells: a role in inflammation and angiogenesis. *Front Biosci* 2005;**10**:1177−82.
51. Feng L, Shi W, Chen Q, Cheng H, Bao J, Jiang C, et al. Smart asymmetric hydrogel with integrated multi-functions of NIR-triggered tunable adhesion, self-deformation, and bacterial eradication. *Adv Healthc Mater* 2021;**10**:e2100784.
52. Castleberry SA, Almquist BD, Li W, Reis T, Chow J, Mayner S, et al. Self-assembled wound dressings silence MMP-9 and improve diabetic wound healing *in vivo*. *Adv Mater* 2016;**28**:1809−17.
53. Shen Y, Xu G, Huang H, Wang K, Wang H, Lang M, et al. Sequential release of small extracellular vesicles from bilayered thiolated alginate/polyethylene glycol diacrylate hydrogels for scarless wound healing. *ACS Nano* 2021;**15**:6352−68.
54. Nourian Dehkordi A, Mirahmadi Babaheydari F, Chehelgerdi M, Raeisi Dehkordi S. Skin tissue engineering: wound healing based on stem-cell-based therapeutic strategies. *Stem Cell Res Ther* 2019;**10**:111.
55. Liu S, Yu J, Zhang Q, Lu H, Qiu X, Zhou D, et al. Dual cross-linked HHA hydrogel supplies and regulates MPhi2 for synergistic improvement of immunocompromise and impaired angiogenesis to enhance diabetic chronic wound healing. *Biomacromolecules* 2020;**21**:3795−806.
56. Moustakas A, Heldin CH. The regulation of TGFbeta signal transduction. *Development* 2009;**136**:3699−714.
57. Cakin MC, Ozdemir B, Kaya-Dagistanli F, Arkan H, Bahtiyar N, Anapali M, et al. Evaluation of the *in vivo* wound healing potential of the lipid fraction from activated platelet-rich plasma. *Platelets* 2020;**31**:513−20.
58. Bao P, Kodra A, Tomic-Canic M, Golinko MS, Ehrlich HP, Brem H. The role of vascular endothelial growth factor in wound healing. *J Surg Res* 2009;**153**:347−58.
59. Gurtner GC, Werner S, Barrandon Y, Longaker MT. Wound repair and regeneration. *Nature* 2008;**453**:314−21.

60. Sheng L, Zhang Z, Zhang Y, Wang E, Ma B, Xu Q, et al. A novel "hot spring"-mimetic hydrogel with excellent angiogenic properties for chronic wound healing. *Biomaterials* 2020;**264**:120414.
61. Wang Y, Lv Q, Chen Y, Xu L, Feng M, Xiong Z, et al. Bilayer hydrogel dressing with lysozyme-enhanced photothermal therapy for biofilm eradication and accelerated chronic wound repair. *Acta Pharm Sin B* 2023;**13**:284−97.
62. Boswell SG, Cole BJ, Sundman EA, Karas V, Fortier LA. Platelet-rich plasma: a milieu of bioactive factors. *Arthroscopy* 2012;**28**:429−39.
63. Teixeira SPB, Domingues RMA, Shevchuk M, Gomes ME, Peppas NA, Reis RL. Biomaterials for sequestration of growth factors and modulation of cell behavior. *Adv Funct Mater* 2020;**30**:1909011.